

Derivation of the Lattice Boltzmann Model for Relativistic Hydrodynamics

M. Mendoza,^{1,*} B. M. Boghosian,^{2,†} H. J. Herrmann,^{1,‡} and S. Succi^{3,§}

¹ *ETH Zürich, Computational Physics for Engineering Materials,*

Institute for Building Materials, Schafmattstrasse 6, HIF, CH-8093 Zürich (Switzerland)

² *Bromfield-Pearson, Medford, Massachusetts 02155, Department of Mathematics, Tufts University*

³ *Istituto per le Applicazioni del Calcolo C.N.R., Via dei Taurini, 19 00185, Rome (Italy),
and Freiburg Institute for Advanced Studies, Albertstrasse, 19, D-79104, Freiburg, Germany*

(Dated: September 2, 2010)

A detailed derivation of the Lattice Boltzmann (LB) scheme for relativistic fluids recently proposed in Ref. [1], is presented. The method is numerically validated and applied to the case of two quite different relativistic fluid dynamic problems, namely shock-wave propagation in quark-gluon plasmas and the impact of a supernova blast-wave on massive interstellar clouds. Close to second order convergence with the grid resolution, as well as linear dependence of computational time on the number of grid points and time-steps, are reported.

PACS numbers: 47.11.-j, 12.38.Mh, 47.75.+f

Keywords: Lattice Boltzmann, quark-gluon plasma, relativistic fluid dynamics, supernovas

I. INTRODUCTION

Relativistic fluid dynamics plays a major role in many fields of modern physics, e.g. astrophysics, nuclear and high-energy physics and, lately, also in condensed matter. The dynamics of such systems requires solving highly nonlinear equations, rendering the analytic treatment of practical problems extremely difficult. Therefore, several numerical methods have been developed, based on macroscopic continuum description [2–4] and kinetic theory[5]. Very recently, a new Lattice Boltzmann (LB) scheme for relativistic fluids has been proposed, and numerically validated for two rather different relativistic applications, shock waves in quark-gluon plasmas and blast waves from supernova explosions impinging against dense interstellar clouds [1]. This fills a missing entry in the remarkably broad spectrum of LB applications across most areas of fluid-dynamics, including quantum fluids [6]. While a quantitative assessment of its practical impact on relativistic fluid dynamics must necessarily await for a long and thorough validation activity, work in Ref. [1] provides robust indications that the relativistic LB (RLB) stands concrete chances of carrying the recognized advantages of LB schemes for classical fluids, over to the relativistic context. We refer primarily to mathematical simplicity/computational efficiency, especially on parallel computers [7], and easy handling of complex geometries.

In this paper, we present an extended version of our previous work [1]. First, we provide full details of the analytical and numerical formulation leading to the relativistic LB scheme, including the asymptotic (Chapman-

Enskog) analysis of the continuum fluid-dynamic limit, starting from the kinetic level. The numerical validation for the case of quark-gluon plasmas is also extended in such a way as to probe the convergence/accuracy of the RLB schemes as a function of grid resolution. Like for classical fluids, second-order convergence and linear scaling of CPU time with number of grid points and time-steps is found. Moreover, the application to supernova blast waves is explored in more detail, by investigating the effect of increasing Lorentz factors on the space-time distribution of the density and pressure fields. Here, the numerical simulation of the relativistic flow past a dense inter-stellar medium (massive clouds) provides a clear indication that sweeping of interstellar matter across the cloud becomes appreciable only for relativistic beta factors $\beta > 0.5$.

II. THE BASIC IDEA

The procedure developed [1] was prompted by two simple observations, i) the kinetic formalism is naturally covariant/hyperbolic, ii) being based on a finite-velocity, discrete (beam) representation of the kinetic distribution function, standard lattice Boltzmann methods naturally feature relativistic-like equations of state, whereby the sound speed, c_s is a sizeable fraction of the speed of light c , i.e. the maximum velocity of mass transport ($c_s/c = K$, with $0.1 < K < 1$). Based on the above, and choosing the lattice speed close to the value of the actual light-speed (at variance with standard LB applications) $c_l \equiv \delta x / \delta t \sim c$, the LB mathematical framework allows the relativistic extension developed in our previous work. The standard LB reads as follows:

$$f_i(\vec{x} + \vec{c}_i \delta t; t + \delta t) - f_i(\vec{x}; t) = -\omega \delta t (f_i - f_i^{eq}) \quad , \quad (1)$$

where $f_i(\vec{x}; t)$ denotes the probability of finding a particle at lattice site \vec{x} and time t , moving along the direction pointed by the discrete velocity \vec{c}_i . The left-hand side

*Electronic address: mmendoza@ethz.ch

†Electronic address: bruce.boghosian@tufts.edu

‡Electronic address: hjherrmann@ethz.ch

§Electronic address: sauro.succi@gmail.com

is readily recognized as an *exact* lattice transcription of the free-streaming term $(\partial_t + v_a \nabla_a)f$ of the continuum Boltzmann equation, where Latin index a labels the spatial coordinates and repeated indices are summed upon. Being naturally covariant, this term goes virtually unchanged over to the relativistic context.

The right-hand-side, on the other hand, is a discrete version of the collision operator, here taking the form of a simple relaxation around a local equilibrium f_i^{eq} , on a timescale $\tau = 1/\omega$. The local equilibrium encodes the symmetries/conservation laws governing the ideal (non-dissipative) fluid regime, namely mass-momentum-energy conservation and Galilean invariance. While molecular details of the collisional processes can be safely foregone, these conservation properties must necessarily be preserved in the lattice formulation.

The discrete local equilibrium is usually expressed as a local Maxwellian, expanded to second order in the local Mach number $Ma = u/c_s$, u being the local flow speed. For the case of athermal flows, this takes the form

$$f_i^{eq} = w_i \rho \left(1 + \frac{c_{ia} u_a}{c_s^2} + \frac{Q_{iab} u_a u_b}{2c_s^4} \right) , \quad (2)$$

where (particle mass is taken to unity for simplicity):

$$\begin{aligned} \rho &= \sum_i f_i , \\ \rho u_a &= \sum_i f_i c_{ia} , \end{aligned}$$

are the fluid density and mass current density, respectively. In the above, w_i is a set of weights, obeying the sum-rules $\sum_i w_i = 1$ and $\sum_i w_i c_{ia}^2 = c_s^2$, and $Q_{iab} = c_{ia} c_{ib} - c_s^2 \delta_{ab}$ is the projector along the i -th spatial direction. It is readily checked that the local equilibria fulfill the following conservation rules

$$\begin{aligned} \sum_i f_i^{eq} &= \sum_i f_i = \rho , \\ \sum_i f_i^{eq} c_{ia} &= \sum_i f_i c_{ia} = \rho u_a , \\ \sum_i f_i^{eq} c_{ia} c_{ib} &= \rho (u_a u_b + c_s^2 \delta_{ab}) . \end{aligned} \quad (3)$$

The first two are the usual mass-momentum conservation laws, whereas the latter ensures the isotropy of the equilibrium momentum-flux. The latter is crucial to secure the proper non-linear structure of the Navier-Stokes equations, and indeed only specific classes of discrete lattices fulfill the aforementioned conservation constraints. As previously noted, lattice equilibria can be obtained by local expansion of the continuum expression of local Maxwell equilibria. In a more empirical way, they could also be obtained by matching the local equilibria in parametric form, $A e^{-B c_{ia} u_a}$, to the conservation rules [8], thereby fixing the Lagrangian parameters A and B in terms of the conserved hydrodynamic fields ρ and u_a .

The possibility of fixing local equilibria by simply expanding the local continuum Maxwellian, which is more elegant than empirical matching [9], is by no means evident.

In fact, it is strictly related to the well-known property of the local Maxwellian to serve as the generating function of Hermite's polynomials H_n (here $v = v/c_s$ and $u = u/c_s$);

$$e^{-\frac{(v-u)^2}{2}} = e^{-\frac{v^2}{2}} \sum_{n=0}^{\infty} H_n(v) u^n . \quad (4)$$

Note that the Galilean invariance manifestly encoded at the right-hand side through the dependence on the magnitude of the relative speed $(v_a - u_a)$, can only be preserved by including *all* terms in the Mach-number expansion at the right hand side. It is quite fortunate that the Navier-Stokes equations only involve quadratic nonlinearities in the flow field, because this allows to develop a consistent lattice hydrodynamic theory by retaining only second order terms in the Mach-number expansion. A similar line of thinking can also be applied to the relativistic equations, with due changes in the mathematical-physical details, to be discussed shortly.

On the other hand, we are not aware of any relativistic analogue of the relation (4) for relativistic local equilibria (Jüttner distribution). Because of this, the relativistic LB scheme has been devised according to the moment-matching procedure discussed above. That is, the local kinetic equilibria are expressed as parametric polynomials of the relativistic fluid velocity $\vec{\beta} = \vec{u}/c$, with the Lagrangian parameters fixed by the condition of matching the analytic expression of the relevant relativistic moments, namely the number density, energy density and energy-momentum. As anticipated, the possibility of a successful matching stems directly from the fact that, even in standard (non-relativistic) LB fluids, the sound speed c_s is of the same order of the speed of light, typically $c_s = c/\sqrt{3}$, which is exactly the equation of state of ideal relativistic fluids. As a result, $|\vec{\beta}| = Ma/\sqrt{3}$, so that $|\vec{\beta}|$ is of the same order as the Mach number $Ma = |\vec{u}|/c_s$. Thanks to this simple, and yet basic property, it is possible to tackle weakly relativistic problems in close analogy with the LB theory of classical low-Mach fluids, the algebraic details being of course quite different in the two cases.

This permits to carry most of the LB formalism over to the context of weakly relativistic fluids, such as quark-gluon plasmas generated by recent experiments on heavy-ions and hadron jets [10–16], as well as astrophysical flows, such as interstellar gas and supernova remnants [17–20].

The RLB scheme is verified through quantitative comparison with recent one dimensional hydrodynamic simulations of relativistic shock wave propagation in viscous quark-gluon plasmas [21], and also applied to the three dimensional case of a blast-wave, produced by a super-

nova explosion, colliding against interstellar massive matter, e.g. molecular gas [17].

Being based on a second-order moment-matching procedure, rather than on a high-order systematic expansion in $\vec{\beta}$ of the local relativistic equilibrium (Jüttner) distribution[5], the RLB is limited to weakly relativistic problems, with $|\vec{\beta}| \sim 0.1$. Note in fact that, unlike the continuum Maxwellian, polynomial expansions are positive-definite only for Mach-number (relativistic β) below a given threshold, typically $Ma \sim 0.3$. However, by introducing artificial faster-than-light particles (numerical “tachyons”), the RLB scheme can be taken up to $|\vec{\beta}| \sim 0.6$, corresponding to Lorentz’s factors $\gamma = \frac{1}{\sqrt{1-|\vec{\beta}|^2}} \sim 1.4$ [1]. Although still far from strongly relativistic regimes, with $\gamma \gg 10$ and higher, this Lorentz factor is nevertheless relevant to a host of important relativistic fluid problems at wildly disparate scales, such as quark-gluon plasmas and relativistic outflows in supernova explosions and possibly even Dirac fluids in graphene [22].

III. MODEL DESCRIPTION

We begin our model description by considering the relativistic fluid equations associated with the conservation of number of particles and momentum-energy. The energy-momentum tensor reads as follows[23, 24]: $T^{\mu\nu} = P\eta^{\mu\nu} + (\epsilon + P)u^\mu u^\nu + \pi^{\mu\nu}$, ϵ being the energy density, P the hydrostatic pressure and $\pi^{\mu\nu}$ the dissipative component of the stress-energy tensor, to be specified later. The velocity 4-vector is defined by $u^\mu = (\gamma, \gamma\vec{\beta})^\mu$, where $\vec{\beta} = \vec{u}/c$ is the velocity of the fluid in units of the speed of light and $\gamma = \frac{1}{\sqrt{1-|\vec{\beta}|^2}}$. The tensor $\eta^{\mu\nu}$ denotes the Minkowski metric. Additionally, we define the particle 4-flow, $N^\mu = n\gamma(1, \vec{\beta})^\mu$, with n the number of particles per volume. Applying the conservation rule to energy and momentum, $\partial_\mu T^{\mu\nu} = 0$, and to the 4-flow, $\partial_\mu N^\mu = 0$, we obtain the hydrodynamic equations,

$$\partial_t ((\epsilon + P)\gamma^2 - P) + \partial_a ((\epsilon + P)\gamma^2 u_a) + \partial_t \pi^{00} + \partial_a \pi^{a0} = 0, \quad (5a)$$

$$\partial_t ((\epsilon + P)\gamma^2 u_b) + \partial_b P + \partial_a ((\epsilon + P)\gamma^2 u_a u_b) + \partial_t \pi^{0b} + \partial_a \pi^{ab} = 0, \quad (5b)$$

for the energy momentum conservation, and

$$\partial_t (n\gamma) + \partial_a (n\gamma u_a) = 0, \quad (6)$$

for the conservation of particle number. Note that, unlike the case of non-relativistic fluids, we have two scalar equations, one for the particle number and one for the energy (in classical hydrodynamics energy appears as the trace of a second-order moment, namely the momentum-flux). To complete the set of equations, we need to define a state equation relating at least two of the three quantities: n , P and ϵ .

A. Relativistic Boltzmann Equation

The above hydrodynamic equations can be derived as a macroscopic limit of the relativistic Boltzmann equation. For the case of a single non-degenerated gas, and in the absence of external forces, this reads as follows[23]:

$$\partial_\mu (p^\mu f) = \int (f'_* f' - f_* f) \Phi \sigma d\Omega \frac{d^3 p_*}{p_{*0}}, \quad (7)$$

where $p^\mu = \left(\frac{E(p)}{c}, \vec{p}\right)$ is the particle 4-momentum with $E(p)$ the relativistic energy as function of the momentum magnitude $p=|\vec{p}|$, $E(p) = (p^2 c^2 + m^2 c^4)^{1/2}$. In the above, $f_* \equiv f(\vec{x}, \vec{p}_*, t)$ and $f \equiv f(\vec{x}, \vec{p}, t)$ denote the distribution functions before the collision, while $f'_* \equiv f(\vec{x}, \vec{p}'_*, t)$ and $f' \equiv f(\vec{x}, \vec{p}', t)$ are the resulting ones after the collision. The base of the so-called collision cylinder is described by $\sigma d\Omega$, with σ the differential cross section, Ω is the solid angle, and

$$\Phi = \frac{p^0 p_*^0}{c} \sqrt{(\vec{v} - \vec{v}_*)^2 - \frac{1}{c^2} (\vec{v} \times \vec{v}_*)^2} = \sqrt{(p^\mu p_\mu)^2 - m^2 c^4} \quad (8)$$

is the Lorentz invariant flux [23], with \vec{v} and \vec{v}_* the velocity of the particles with momentum \vec{p} and \vec{p}_* , respectively. The right-hand-side of Eq. (7) is the collision term, whose details fix the value of the transport coefficients in the macroscopic equations. Although the collision integral can be expressed in terms of the second kind modified Bessel functions and numerical integrations [23], simpler expressions have been proposed, along the lines of the BGK (Bhatnagar-Gross-Krook) approximation for non-relativistic fluids. The first relativistic BGK (RBGK), as proposed by Marle[25], reads as follows:

$$\partial_\mu (p^\mu f) = \frac{m}{\tau_M} (f^{eq} - f), \quad (9)$$

where f^{eq} is a local relativistic equilibrium, m is the particle rest mass, and τ_M represents a characteristic time between subsequent collisions. This can be regarded as the relaxation time only in a local rest frame where the momentum of the particles is zero[23]. It is well-known that in a general inertial frame, the relaxation time $\hat{\tau}_M$ can be written as follows:

$$\hat{\tau}_M = \frac{p^0}{mc} \tau_M. \quad (10)$$

Although, in the Marle model, the transport coefficients are expressed usually as functions of the characteristic time τ_M , they cannot be described as functions of the relaxation time $\hat{\tau}_M$ because it depends on the microscopic momentum component p^0 , which means on microscopic $\gamma_v = \frac{1}{\sqrt{1-|\vec{v}|^2/c^2}}$, and therefore it cannot appear

in any macroscopic description. To avoid this problem, Takamoto and Inutsuka [26] proposed a modified Marle

model, in which the relaxation time τ is taken as the weighted average, i.e. $\frac{1}{\tau} = \langle \frac{1}{\tau_M} \rangle$. With this approximation, the following relation can be obtained [23, 26]

$$\tau_M = \frac{K_1(\chi)}{K_2(\chi)} \tau \quad , \quad (11)$$

where $\chi \equiv \frac{mc^2}{kT}$ and K_n is the second kind modified Bessel function of order n . The correction $\frac{K_1(\chi)}{K_2(\chi)}$ tends to 1 at low temperatures, i.e. $\chi \rightarrow \infty$, and to $\frac{\chi}{2}$ in the limit of high temperatures, i.e. $\chi \rightarrow 0$. In this modified approach, the characteristic time in the transport coefficient can be replaced by the relaxation time τ using Eq. (11) as an approximation.

The Marle model provides a good approximation of the full collision term at low temperatures.

A more general RBGK model, which provides a reasonable approximation of the transport coefficients at both low and high temperatures, was subsequently proposed by Anderson and Witting [27], and it reads as follows:

$$\partial_\mu(p^\mu f) = \frac{u^\mu p_\mu}{c^2 \tau_A} (f^{eq} - f) \quad , \quad (12)$$

τ_A being the relaxation time.

Both models can reproduce on the macroscopic level the conservation equations given by $\partial_\mu T^{\mu\nu} = 0$, and $\partial_\mu N^\mu = 0$, although with different expressions for the dissipative terms and transport coefficients. For instance, the shear viscosity using the Marle model is given by $\eta_M \simeq \frac{4P^{eq}\tau_M}{\chi}$ for high temperatures (ultra-relativistic case), with P^{eq} the equilibrium pressure, while with the Anderson-Witting model yields $\eta_A \simeq \frac{4P^{eq}\tau_A}{5}$.

In general, the dissipation parameters, like the bulk viscosity, thermal conductivity and shear viscosity, are only approximations of the values obtained by linearization of the full collision term in the relativistic Boltzmann equation, Eq.7.

Having discussed the BGK formulation in the relativistic context, we next proceed to map it within the Lattice Boltzmann framework.

B. Lattice Boltzmann Model

The Lattice Boltzmann theory for classical fluids shows that it may prove more convenient to solve fluid problems by numerically integrating the underlying kinetic equation rather than the macroscopic fluid equation themselves. The main condition for this to happen is that a sufficiently economic representation of the velocity degrees of freedom be available. Following upon consolidated experience with non-relativistic fluids, such a representation is indeed provided by discrete lattices, whereby the particle velocity (momentum) is constrained to a handful of constant discrete velocities, with sufficient symmetry to secure isotropy and the fundamental conservations of fluid flows, namely mass-momentum-energy

conservation and rotational invariance. The main advantages of the kinetic representation of classical fluids have been discussed at length [28], and they amount basically to the fact that the information is transported along straight-streamlines (the discrete velocities are constant in space and time) rather than along space-time dependent trajectories generated by the flow itself, as it is case for hydrodynamic equations. Moreover, diffusive transport is not described by second-order spatial derivatives, but rather emerges as a collective property from the adiabatic relaxation of the momentum flux tensor to its local equilibrium value. This is crucial in securing a balance between first-order derivatives in both space and time, which is essential for relativistic equations.

In order to reproduce the relativistic hydrodynamic equations, an LB model with the D3Q19 (19 speeds in 3 spatial dimensions) cell configuration, as shown in Fig. 1, was proposed in Ref. [1]. From Fig. 1 it is readily appreciated that the highest D3Q19 speed is $\sqrt{2}c_l$, $c_l = \frac{\delta x}{\delta t}$ being the limiting lattice speed along each direction. The velocity units are rescaled such that the speed of light becomes $c=1$.

As noted above, relativistic hydrodynamics evolves two scalars, number and energy density. It is therefore convenient to introduce two separate distribution functions f_i and g_i for each velocity vector \vec{c}_i , representing, so to say, “fluons” and “phonons”, respectively.

The hydrodynamic variables are calculated by using the following five macroscopic constraints,

$$n\gamma = \sum_{i=0}^{18} f_i \quad , \quad (13a)$$

$$(\epsilon + P)\gamma^2 - P = \sum_{i=0}^{18} g_i \quad , \quad (13b)$$

$$(\epsilon + P)\gamma^2 \vec{u} = \sum_{i=0}^{18} g_i \vec{c}_i \quad , \quad (13c)$$

From these equations, we need to extract six physical quantities, namely n , \vec{u} , ϵ and P . With five equations for six unknowns, the problem is closed by choosing an equation of state, which we take of the form $\epsilon=3P$ [23]. We wish to emphasize that the present LB scheme is by no means limited to this choice.

Both distribution functions f_i and g_i are postulated to evolve according to the relativistic Boltzmann-BGK equation *based on the low-temperature Marle model*, Eq. (9).

To obtain the lattice analogue of the Marle model, we first write explicitly Eq. (9) as follows:

$$\partial_0(p^0 f) + \partial_a(p^a f) = \frac{m}{\tau_M} (f^{eq} - f) \quad . \quad (14)$$

Replacing the value of the four-momentum, we obtain

$$\partial_0(m\gamma_v f) + \partial_a(mc^a \gamma_v f) = \frac{m}{\tau_M} (f^{eq} - f) \quad , \quad (15)$$

with γ_v the Lorentz factor for the microscopic velocities c^a . Due to the fact that the velocity and spatial coordinates are linearly independent, we can further write:

$$\gamma_v \partial_0 f + \gamma_v c^a \partial_a f = \frac{f^{\text{eq}} - f}{\tau_M} \quad . \quad (16)$$

Dividing by γ_v on both sides of Eq. (16), we obtain

$$\partial_0 f + c^a \partial_a f = \frac{mc}{\tau_M p^0} (f^{\text{eq}} - f) \quad , \quad (17)$$

and replacing Eq. (10), we obtain

$$\partial_0 f + c^a \partial_a f = \frac{1}{\hat{\tau}_M} (f^{\text{eq}} - f) \quad . \quad (18)$$

According to the modified Marle model [26], we can write Eq. (18) as

$$\partial_0 f + c^a \partial_a f = \left(\frac{1}{\tau} - \vartheta \right) (f^{\text{eq}} - f), \quad (19)$$

where the correction term ϑ , using Eq. (11), is given by

$$\begin{aligned} \vartheta &= \left[\left\langle \frac{1}{\tau_{M*}} \right\rangle - \frac{1}{\tau_{M*}} \right] \\ &= \frac{1}{\tau_M} \left[\frac{K_1(\chi)}{K_2(\chi)} - \frac{1}{\gamma_v} \right] \quad . \end{aligned} \quad (20)$$

For low temperatures, $\frac{K_1(\chi)}{K_2(\chi)} \sim 1$ and $\gamma_v \sim 1$, so that the correction term ϑ tends to zero, thereby reconstituting the non-relativistic Boltzmann equation. At high temperatures, this term can be approximated by

$$\vartheta \sim \frac{\chi}{2} \frac{1}{\tau_M} \quad , \quad (21)$$

which also tends to vanish as temperature is made higher.

As noted above, Eq. (19), without the term ϑ , is just the Boltzmann equation for the case of non-relativistic fluids, with the collision time τ representing a realistic relaxation time of the system.

Therefore, for the purpose of this work, we postulate the discrete distribution functions to evolve according to the following pair of BGK Boltzmann equations [29],

$$f_i(\vec{x} + \vec{c}_i \delta t, t + \delta t) - f_i(\vec{x}, t) = -\frac{\delta t}{\tau} (f_i - f_i^{\text{eq}}) \quad , \quad (22)$$

and,

$$g_i(\vec{x} + \vec{c}_i \delta t, t + \delta t) - g_i(\vec{x}, t) = -\frac{\delta t}{\tau} (g_i - g_i^{\text{eq}}) \quad , \quad (23)$$

where f_i^{eq} and g_i^{eq} are the equilibrium distribution functions.

To find the equilibrium distribution functions recovering the relativistic fluid equations, Eqs. (5) and (6), in the continuum limit, we use the moment-matching procedure described earlier on in this paper.

More precisely, we write the equilibrium distribution functions as,

$$f_i^{\text{eq}} = w_i [A + \vec{c}_i \cdot \vec{B}] \quad , \text{ for } i \geq 0 \quad , \quad (24a)$$

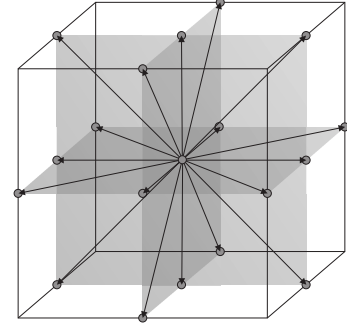


FIG. 1: Set of discrete velocities for the relativistic lattice Boltzmann model. The highest speed is $\sqrt{2}c_l$.

$$g_i^{\text{eq}} = w_i [C + \vec{c}_i \cdot \vec{D} + \vec{E} : (\vec{c}_i \vec{c}_i - \alpha \vec{I})] \quad , \text{ for } i > 0 \quad , \quad (24b)$$

$$g_0^{\text{eq}} = w_0 [F] \quad , \quad (24c)$$

where $\alpha, A, \vec{B}, C, \vec{D}, \vec{E}$ and F are Lagrange parameters, to be fixed by matching the discrete to the correct continuum equations. The weights w_i for this set of discrete speeds are defined by $w_0 = 1/3$ for the rest particles, $w_i = 1/18$ for the velocities $|\vec{c}_i| = c_l$, and $w_i = 1/36$ for $|\vec{c}_i| = \sqrt{2}c_l$.

First, we find the values for A and \vec{B} to obtain the conservation of particle number, Eq. (6). To this purpose, we impose

$$\sum_{i=0}^{18} f_i^{\text{eq}} = n\gamma \quad , \quad (25)$$

and,

$$\sum_{i=0}^{18} f_i^{\text{eq}} \vec{c}_i = n\gamma \vec{u} \quad . \quad (26)$$

Replacing the Eq. (24) into the sums, we arrive to

$$\sum_{i=0}^{18} f_i^{\text{eq}} = A = n\gamma \quad , \quad (27)$$

and

$$\sum_{i=0}^{18} f_i^{\text{eq}} \vec{c}_i = \frac{3}{c_l^2} \vec{B} = n\gamma \vec{u} \quad , \quad (28)$$

where, we can see easily that $A = n\gamma$ and $\vec{B} = \frac{3}{c_l^2} n\gamma \vec{u}$. Next, we have to obtain the Eq. (5) from the equilibrium distribution functions g_i^{eq} . To this end, we impose the following constraints:

$$\sum_{i=0}^{18} g_i^{\text{eq}} = \gamma^2 (\epsilon + P) - P \quad , \quad (29)$$

$$\sum_{i=0}^{18} g_i^{\text{eq}} \vec{c}_i = (\epsilon + P) \gamma^2 \vec{u} \quad . \quad (30)$$

and additionally,

$$\sum_{i=0}^{18} g_i^{\text{eq}} c_{ia} c_{i\beta} = P \delta_{ab} + (\epsilon + P) \gamma^2 u_a u_b \quad . \quad (31)$$

Using a similar procedure as before, we can find the rest of the Lagrange parameters, $\alpha = \frac{c_l^2}{3}$, $C = \frac{3P}{c_l^2}$, $\vec{D} = \frac{3}{c_l^2} (\epsilon + P) \gamma^2 \vec{u}$, $E_{ab} = \frac{9}{2c_l^4} (\epsilon + P) \gamma^2 u_a u_b$, and $F = (\epsilon + P) \gamma^2 \left[3 - 3 \frac{(2+c_l^2)P}{c_l^2(\epsilon+P)\gamma^2} - \frac{3}{2c_l^2} (\epsilon + P) \gamma^2 |\vec{u}|^2 \right]$. These calculations are shown in detail in Appendix A.

The equilibrium distribution functions recovering the relativistic fluid equations in the continuum limit, finally read as follows:

$$f_i^{\text{eq}} = w_i n \gamma \left[1 + 3 \frac{(\vec{c}_i \cdot \vec{u})}{c_l^2} \right] \quad , \quad (32)$$

for $i \geq 0$,

$$g_i^{\text{eq}} = w_i (\epsilon + P) \gamma^2 \left[\frac{3P}{(P + \epsilon) \gamma^2 c_l^2} + 3 \frac{(\vec{c}_i \cdot \vec{u})}{c_l^2} + \frac{9}{2} \frac{(\vec{c}_i \cdot \vec{u})^2}{c_l^4} - \frac{3}{2} \frac{|\vec{u}|^2}{c_l^2} \right] \quad , \quad (33)$$

for $i > 0$, and

$$g_0^{\text{eq}} = w_0 (\epsilon + P) \gamma^2 \left[3 - \frac{3P(2 + c_l^2)}{(P + \epsilon) \gamma^2 c_l^2} - \frac{3}{2} \frac{|\vec{u}|^2}{c_l^2} \right] \quad , \quad (34)$$

for the rest particles.

By Taylor expanding the Eqs. (22) and (23) to second order in δt , and retaining terms only up to first order in the Chapman-Enskog expansion $f = f^{\text{eq}} + \kappa f^1 + \dots$, where $\kappa \sim c \tau \nabla$ is the Knudsen number, the LB equations can be shown to reproduce the following continuum fluid equations as derived in detail in Appendix B:

$$\partial_t [(\epsilon + P) \gamma^2 - P] + \partial_a [(\epsilon + P) \gamma^2 u_a] = 0 \quad , \quad (35a)$$

$$\begin{aligned} \partial_t [(\epsilon + P) \gamma^2 u_b] + \partial_b P + \partial_a [(\epsilon + P) \gamma^2 u_a u_b] \\ = \partial_a [\partial_b (\eta \gamma u_a) + \partial_a (\eta \gamma u_b) + \partial_l (\eta \gamma u_l) \delta_{ab}] , \end{aligned} \quad (35b)$$

for the energy momentum conservation, and

$$\partial_t (n \gamma) + \partial_a (n \gamma u_a) = 0 \quad , \quad (36)$$

for the conservation of particle number. The indices a, b and l denote the spatial components.

The choice of the state equation, $\epsilon = 3P$, simplifies the equilibrium functions as follows,

$$f_i^{\text{eq}} = w_i n \gamma \left[1 + 3 \frac{(\vec{c}_i \cdot \vec{u})}{c_l^2} \right] \quad , \quad (37)$$

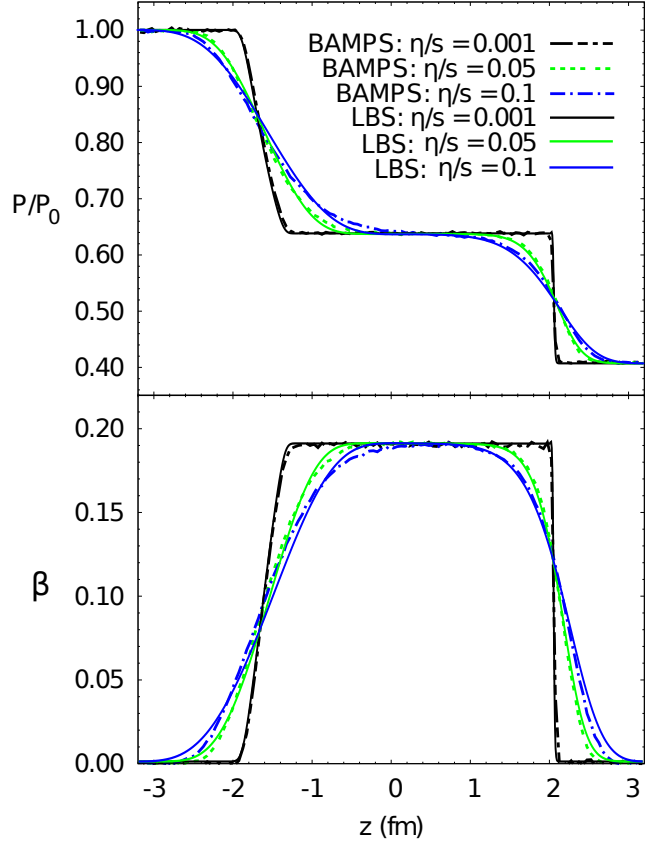


FIG. 2: Comparison between the BAMPS simulations[21] and the lattice Boltzmann results at $t=3.2\text{fm}/c$. Note that, in both simulations, the value of $\beta \sim 0.2$ for the speed of propagation of the shock wave is obtained. Pressure (top) and velocity (bottom) of the fluid as function of the spatial coordinate z .

for $i \geq 0$ and,

$$g_i^{\text{eq}} = w_i \epsilon \gamma^2 \left[\frac{1}{\gamma^2 c_l^2} + 4 \frac{(\vec{c}_i \cdot \vec{u})}{c_l^2} + 6 \frac{(\vec{c}_i \cdot \vec{u})^2}{c_l^4} - 2 \frac{|\vec{u}|^2}{c_l^2} \right] \quad (38)$$

for $i > 0$ and,

$$g_0^{\text{eq}} = w_0 \epsilon \gamma^2 \left[4 - \frac{2 + c_l^2}{\gamma^2 c_l^2} - 2 \frac{|\vec{u}|^2}{c_l^2} \right] \quad , \quad (39)$$

for $i=0$. Then, the equations for the macroscopic variables take the form: $n \gamma = \sum_{i=0}^{18} f_i$, $\frac{4}{3} \epsilon (\gamma^2 - \frac{1}{4}) = \sum_{i=0}^{18} g_i^p$ and $\frac{4}{3} \epsilon \gamma^2 \vec{u} = \sum_{i=0}^{18} g_i \vec{c}_i$. The shear viscosity is computed as $\eta = \frac{4}{9} \gamma \epsilon (\tau - \delta t/2) c_l^2$.

Also, it is worth noting that our scheme smoothly recovers the non-relativistic limit by simply letting $\beta \rightarrow 0$.

IV. DISSIPATIVE HYDRODYNAMICS

According to kinetic theory, dissipative effects emerge at the level of first order terms in the Knudsen number

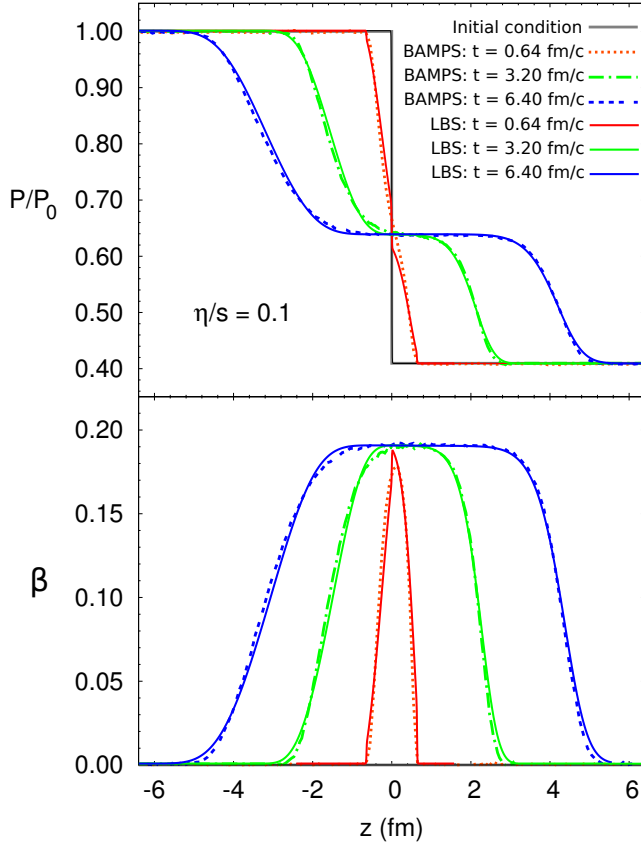


FIG. 3: Time evolution of the shock wave for BAMPs simulations[21] and Lattice Boltzmann results. Here the speed of propagation of the shock wave $\beta \sim 0.2$ is obtained.

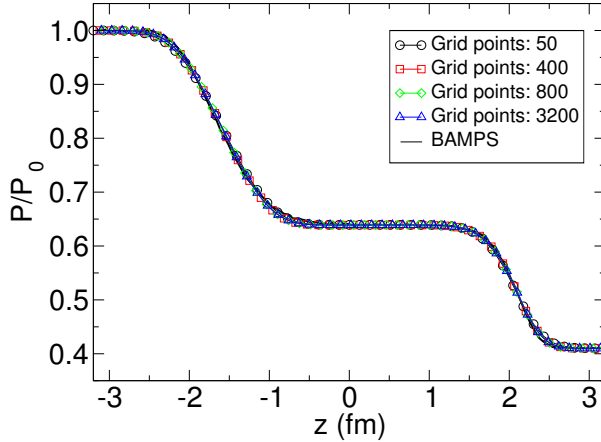


FIG. 4: Lattice Boltzmann simulation of the shock wave for different grid resolutions, $\beta \sim 0.2$ and $\eta/s = 0.05$.

expansion of the kinetic equations. At a more fundamental level, dissipation is an emergent property resulting from the finite-time relaxation of non-equilibrium kinetic excitations on top of the hydrodynamic "ground state". A detailed Chapman-Enskog analysis (see Appendix B), shows that the lattice formulation needs to retain second order terms in the lattice spacing, which means that the

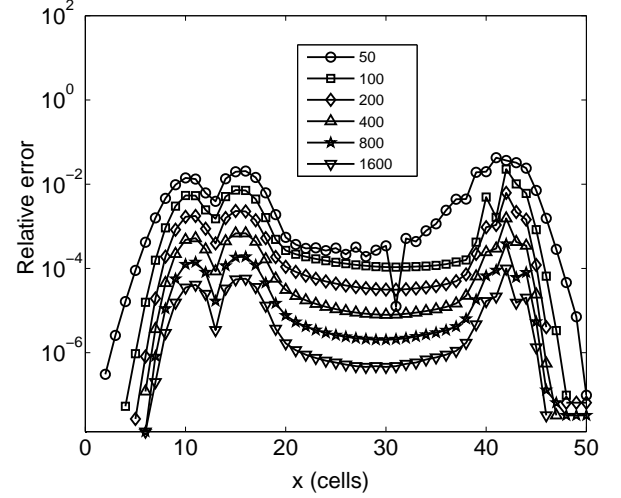


FIG. 5: Relative convergence error for different grid resolutions as a function of the x -coordinate for $\beta \sim 0.2$ and $\eta/s = 0.01$.

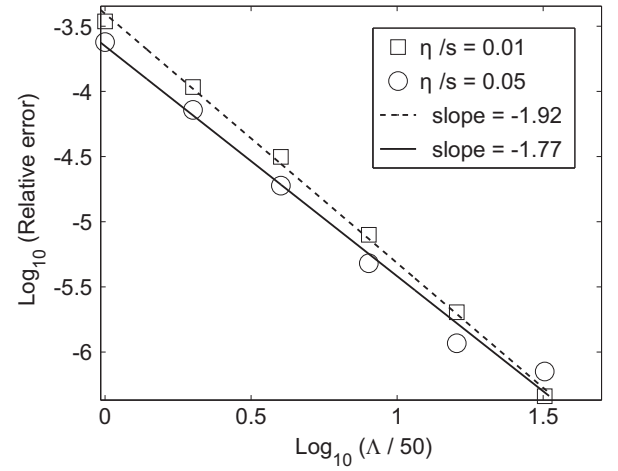


FIG. 6: Relative convergence error as a function of the number of grid points, for $\beta \sim 0.2$. Λ represents the number of grid points. Here, the relative error E_{ave} is calculated by taken the mean value of the relative errors at every location z , $E_{ave} = \frac{1}{\Lambda} \sum_{z=1}^{\Lambda} E_r(z)$.

streaming operator needs to be expanded to second order in the lattice time step δt and, by the light-cone rule, in δx too. Straightforward but lengthy algebra, leads to the following expression of the LB dynamic viscosity [30]

$$\eta = \rho c_s^2 \left(\tau - \frac{\delta t}{2} \right) \equiv \rho c_s^2 \tau \left(1 - \frac{\theta}{2} \right), \quad (40)$$

where we have defined

$$\theta = \frac{\delta t}{\tau}, \quad (41)$$

as the parameter measuring the time-granularity of the LB scheme. Indeed, the limit $\theta \rightarrow 0$ reproduces the continuum value $\eta = \rho c_s^2 \tau$. Similar calculations for the relativistic case yield (see more details in Appendix B)

$$\eta = \gamma c_s^2 \tau (\epsilon + P)(1 - \theta/2) c_l^2. \quad (42)$$

A few comments are in order. First, we note that positivity of the kinematic viscosity implies

$$0 < \theta < 2 \quad (43)$$

This linear stability constraint for the discrete scheme, is readily seen to associate with the second-principle (negative viscosity implies physical instability).

The above expressions seem to suggest that ideal hydrodynamics, i.e. strictly zero dissipation, could be achieved in the limit $\delta t \rightarrow 2\tau$, i.e. $\theta \rightarrow 2$. Actual practice, though, shows that this limit is an illusory one, since, whenever the viscosity falls below a given (flow-dependent) threshold, the stability of the scheme is compromised. Physically, the reason is that below a given threshold, the system is no longer capable of dissipating short-scale gradients, thereby allowing the non-equilibrium component of the distribution function to grow wildly, and finally ruin the simulation. This is in line with the so-called “numerical uncertainty principle” (NUP) for transport advection equations, according to which a minimum non-zero viscosity is required to secure the positivity of the positive-definite quantities, such as the fluid density [31]. In a nutshell, the point is that, in order to reach zero viscosity with a positive definite distribution, wavelengths at *all* scales are needed, including those below the lattice spacing δx . Since - by construction- the latter are missing from a discrete lattice representation, positivity can only be maintained through a finite amount of dissipation, typically of the order of the inherent lattice viscosity $\frac{\delta x^2}{\delta t}$. Incidentally, we note that viscosity has the same physical dimension as $\delta x \delta v \sim \hbar/m$, whence the notion of “uncertainty principle”.

For LB equations, the NUP can be formulated in terms of an inequality involving the equilibrium and non-equilibrium components of the discrete distribution function. To appreciate this point, let us first recast the standard LB in the following collide-stream form:

$$f_i(\vec{x} + \vec{c}_i \delta t; t + \delta t) = f'_i(\vec{x}; t) \equiv (1 - \theta) f_i(\vec{x}; t) + \theta f_i^{eq} \quad (44)$$

where f' denotes the so-called post-collisional distribution function.

From the above, it is seen that positivity of the post-collisional distribution at time t guarantees positivity of the distribution at the subsequent time $t + \delta t$. Simple algebra yields:

$$\theta < \theta_{NUP}[f] \equiv \min_i \left\{ \frac{|f_i^{eq}|}{|f_i^{neq}|} \right\}$$

This informative expression suggests the definition of three distinct non-equilibrium regimes:

1. Weak non-equilibrium ($\theta_{NUP} > 2$)
2. Strong non-equilibrium ($1 < \theta_{NUP} < 2$)
3. Extreme non-equilibrium ($\theta_{NUP} < 1$)

In the weak non-equilibrium regime (often referred to as strong-coupling regime), the one relevant to hydrodynamics, the NUP does not set any additional constraint to linear stability. In the strong non-equilibrium regime, however, non-linear stability may in principle set the most stringent constraint. Clearly, this is even more so in the extreme non-equilibrium region, where the non-equilibrium component exceeds the equilibrium one, in total defiance of hydrodynamics.

Remarkably, LB proves capable of stable operation in this “linearly-forbidden” region. In fact, the negative shift $-\delta t/2$, (“propagation viscosity” in LB jargon) which stems directly from the light-cone structure of the LB streaming operator, permits to attain very small viscosities, of order, say, 10^{-3} in lattice units, while still keeping $\delta t = 1$, and $\theta \sim 2 - O(10^{-3})$. This allows for the simulation of very-low viscous flows (such as the quark-gluon plasma) with time-steps of order $O(1)$, which proves very beneficial for computational purposes.

The ultimate reason for such favorable behavior in the strong non-equilibrium regime can be traced to the existence of lattice versions of the H-theorem [32, 33].

Another remarkable property of the LB formulation is that, in contrast to hydrodynamic formulations, dissipation is not represented explicitly through second-order spatial derivatives, but emerges instead from a first-order, covariant *propagation-relaxation* dynamics, through adiabatic enslaving of the momentum-flux tensor to its equilibrium (ideal-hydrodynamic) expression. As a result of this first-order dynamics, the CFL (Courant-Friedrichs-Lewy) stability condition of the LB scheme reads simply as $u \delta t \leq \delta x$, instead of $\nu \delta t < \delta x^2$, the latter being much more demanding on the time-step δt , as the grid is refined ($\delta x \rightarrow 0$). In the above, $\nu = \frac{\mu}{\rho}$ is the fluid kinematic viscosity.

Also to be noted, built-in causality is secured by the hyperbolic structure of the underlying kinetic theory.

Before closing this section, we wish to emphasize that the structure of the dissipative terms could be enriched by turning to a multi-time relaxation version of the collision operator, whereby different moments relax with different rates to their equilibrium expression [34, 35]. This allows to enlarge the list of transport coefficients, including bulk viscosity, thermal conductivity and anisotropic transport parameters.

V. VALIDATION AND APPLICATIONS

Having discussed the basic aspects of the relativistic Lattice Boltzmann theory, we next move on to its numerical validation and application to two different problems of

modern relativistic hydrodynamics, namely shock propagation in viscous quark-gluon plasmas and blast-waves from supernova explosions in interstellar media.

A. Quark-Gluon Plasma

To test the model, we solve the Riemann problem in viscous gluon matter[21] with a ultra-relativistic equation of state $\epsilon=3P$, as before, and the relation between energy density and particle number density, $\epsilon=3nT$, T being the temperature[23]. The initial configuration consists of two regions, divided by a membrane located at $z=0$. Both regions are thermodynamically equilibrated, at different constant pressure, P_0 for $z<0$ and P_1 for $z>0$. At $t=0$, the membrane is removed and the fluid starts expanding.

We implement a one-dimensional simulation with an array of size $1\times 1\times 800$ using open boundary conditions at the two ends of this 1D chain. In this case, the 4-velocity is given by $u^\mu=(\gamma, 0, 0, \gamma\beta)^\mu$. The velocity of the lattice is chosen $c_l=1.0$, so that the cell size δx and time step δt are both fixed to unity. This corresponds in IS units to $\delta x=0.008\text{fm}$ and $\delta t=0.008\text{fm}/c$. The viscosity is calculated as $\eta=\frac{4}{9}\gamma\epsilon(\tau-1/2)$, and the entropy density by the approximation $s=4n-n\ln\lambda$, with $\lambda=\frac{n}{n^{eq}}$ the gluon fugacity. The equilibrium particle density n^{eq} is given by, $n^{eq}=\frac{d_G T^3}{\pi^2}$ with $d_G=16$ for gluons. Next, we calculate the ratio between the viscosity and entropy density, η/s , that is used as a parameter to characterize the conditions for the onset of shock-waves. The pressures were chosen as $P_0=5.43\text{GeVfm}^{-3}$ and $P_1=2.22\text{GeVfm}^{-3}$, corresponding to 7.9433×10^{-6} and 3.2567×10^{-6} in numerical units, respectively. The initial temperature is $T_0=350\text{MeV}$, corresponding to $T_0=0.0287$ in numerical units. With these parameters, the conversion between physical and numerical units for the energy, is $1\text{MeV}=8.2\times 10^{-5}$.

Fig. 2 shows the results for different values of η/s and the comparison with the BAMPS[36] (Boltzmann Approach of Multiparton Scattering) microscopic transport model simulations[21] at time $3.2\text{fm}/c$. Fig. 3, shows the time evolution of the system for $\eta/s=0.1$ for the two numerical models. In both cases, excellent agreement with BAMPS is observed. Fluids moving at higher speed, $\beta\sim 0.6$, were also considered in Ref. [1], where numerical “tachyons” with $c_l=10$ were used.

Indeed, from Eqs. (32) and (33), we see that the positivity condition, $f_i^{eq}>0$, implies $\vec{c}_i \cdot \vec{u} < \frac{c^2}{3}$. As a result, by raising c_l , e.g. by reducing the time-step accordingly, positivity can be preserved for higher values of β .

To check the convergence of the model, we implement simulations taking $\eta/s=0.05$ and $\eta/s=0.01$ for different grid resolutions. Fig. 4 reports the pressure profile at time $3.2\text{fm}/c$ and shows very small differences between the results when the resolution is changed from 50 to 3200 grid points with $\eta/s=0.05$. To obtain a more quantitative measure of the convergence we use the Richardson extrapolation method [37, 38]. In this method, given any quantity $A(\delta x)$ that depends on a size step δx , we

Grid points	Total time steps	CPU time (ms)
50	25	0.94
100	50	3.5
200	100	17.1
400	200	68.4
800	400	272
1600	800	1095
3200	1600	4396

TABLE I: Computational time required for the simulation of the shock waves in quark-gluon plasma as a function of the grid resolution.

can make an estimation of order n of the exact solution A by using

$$A = \lim_{\delta x \rightarrow 0} A(\delta x) \approx \frac{2^n A\left(\frac{\delta x}{2}\right) - A(\delta x)}{2^n - 1} + O(\delta x^{n+1}) \quad , \quad (45)$$

with errors $O(\delta x^{n+1})$ of order $n+1$. Thus the relative error between the value $A(\delta x)$ and the “exact” solution A can be calculated by

$$E_r(\delta x) = \left| \frac{A(\delta x) - A}{A} \right| \quad . \quad (46)$$

In our case, the quantity A is the pressure $P(z)$ and we set up $n=2$. We can estimate the relative error as shown in Fig. 5 for $\eta/s=0.01$ using Eqs. (45) and (46), at every grid point. Indeed, the relative error with respect to the “exact solution” decreases rapidly with increasing grid resolution. More precisely, Fig. 6 shows that the present scheme exhibits a near second-order convergence. This is basically in line with the convergence properties of non-relativistic LB schemes.

However, we can see that for higher viscosity, i.e. larger values of the relaxation time τ , and higher grid resolution (smaller δx), the order of convergence decreases due to the lack of adiabaticity associated with increasing Knudsen number. Nevertheless, the model is still able to reproduce shock waves, at low resolution, hence with a very modest computational time. For instance, using a resolution of 50 grid points, the simulation took 0.94ms in a standard PC. Other values are shown in Table I. From this table, it is readily appreciated that the computational cost scales linearly with the number of grid points and time-steps.

B. Supernova explosion simulation

Several important astrophysical phenomena involve strongly-relativistic hydrodynamics, and some of them fall in the region of $\gamma \sim 1.4$, covered by our scheme. This is the case, for instance, of blastwaves produced by supernova explosions [20]. In this section, we simulate a shock wave, generated by, say, a GRB (γ -ray burst) or XRF (X -ray flash) supernova explosion [19, 20], colliding against an interstellar cloud composed by massive matter, e.g.

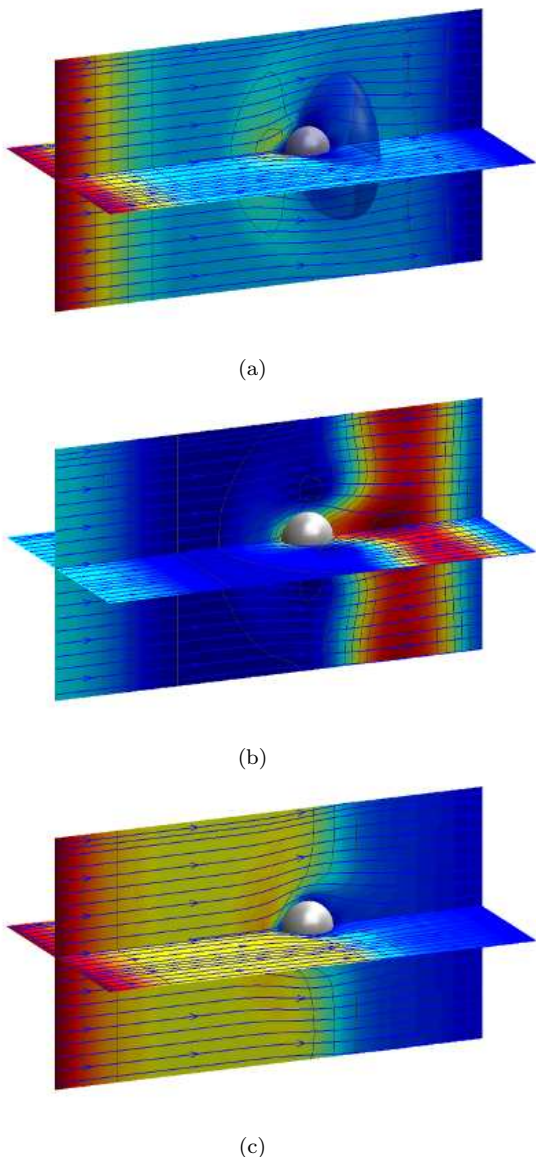


FIG. 7: Relativistic shock wave, generated by a γ -ray burst or X-ray flash supernova explosion [19, 20], impacting on a massive interstellar cloud at $|\vec{\beta}| = 0.5$ at $t = 1350$ time steps which is equivalent to 4280 years. Here the streamlines represent the velocity field, and the colors (a) the pressure, (b) the particles density, and (c) the temperature. The simulation was implemented on a grid of $200 \times 100 \times 100$ cells.

molecular gas[17]. The ejecta from the explosion of such supernovae are known to sweep the interstellar material along, up to relativistic velocities (relativistic outflows) [18–20].

The simulation is implemented in a box of size $6 \times 3 \times 3 \times 10^{16}$ Km in a coordinate system (x, y, z) , using a lattice of $200 \times 100 \times 100$ cells, which gives a cell length $\delta x = \delta y = \delta z = 3 \times 10^{14}$ Km, using numerical “tachyons” with $c_l = 10$, and a time step $\delta t = 3.17$ years. The simulation region is divided in two zones by the plane $x = 50$. The interstellar medium, located at $x > 50$, is character-

ized by a particle density $n_1 = 0.6 \text{ cm}^{-3}$ and temperature $T_1 = 10^4$ K. The massive cloud is modeled as a spherical obstacle, with a radius of 10 cells, centered at location (100, 50, 50). The boundary condition on the surface of the obstacle is implemented forcing the obstacle cells to evolve to the equilibrium distribution function with the constant values, $n = n_1$, $\vec{u} = 0$, and $T = T_1$. Open boundary condition was implemented at right, left, top, bottom and front of the simulation zone according to the shock wave propagation direction (x -direction), which consists on copying the information of the distribution functions from the second last cells to the last ones of the boundary. At back boundary we set an inlet flow boundary condition fixing the distribution functions of the boundary cells with the equilibrium distribution function evaluated with the initial conditions n_0 and T_0 [30, 39]. In order to obtain a shock wave moving at $|\vec{\beta}| \simeq 0.5$ along the x -direction, we set $T_0 = 6T_1$ and $n_0 = 2n_1$ for the region $x \leq 50$. The simulation, spanning 1350 time steps, takes about 1900 CPU seconds on a standard PC. Fig. 7 shows the simulation results for the velocity, pressure, particle density, and temperature fields of the supernova remnant, during the impact of the shock wave on the massive interstellar cloud, red and blue denoting high and low values, respectively.

Here, we can see that the density n is higher in the shock front, due to sweeping of interstellar material by the shock-wave, which is compressing the fluid. On the other hand, the temperature of the fluid is higher in the zone of $x \leq 50$, as a consequence of the initial configuration. The temperature is seen to increase in the zone where the collision takes place (see Fig. 8), and so does the temperature. This is due to conversion of kinetic energy to pressure/temperature caused by the momentum lost on the solid boundary of the massive cloud.

Fig. 8 illustrates in more detail the density n , pressure P and temperature T of the fluid during the collision and compares the respective curves with the ones obtained when the obstacle is absent. Note that the particle density, pressure, and temperature values, with and without obstacle, present a small difference sufficiently downstream the obstacle along the x -axis at $y = z = 50$ (see Fig. 8). During the collision, the shockwave surrounds the obstacle and later the fluid meets again at the x -axis and overlaps. Due to this, the x -component of the shockwave propagation velocities are the same (because of symmetry) for all the incoming fluid to the meeting zone, the perturbations along this axis close to the shock front are weak, contrary to the zone near the obstacle, where the fluid fills up again, due to the low pressure. However, the fluid moves slower than in the case without obstacle because of the existence of flow moving outwards off the axis. If we increase the ratio between the cross section and the length of the obstacle, larger departures between the velocity of the shock-fronts with and without obstacle would be expected. Moreover, later in time after the collision, differences in the pressure and other quantities, can generate turbulence. Transversal perturbations

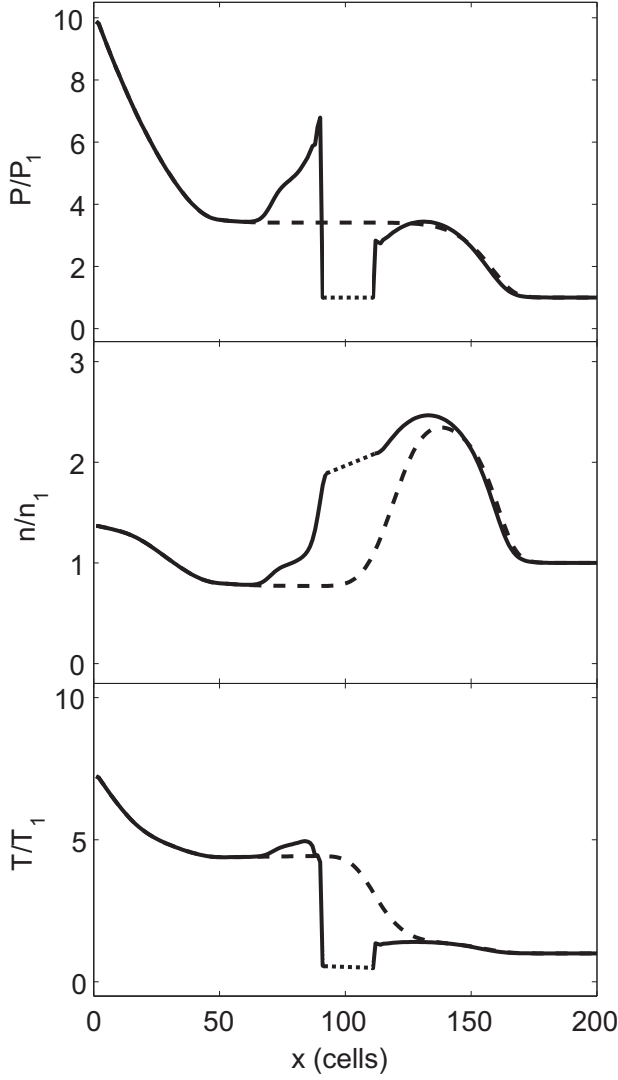


FIG. 8: Pressure P , number of particles density n , and temperature T of the supernova remnant as a function of the x coordinate at $y = z = 50$ and $t = 1350$ time steps equivalent to 4280 years. The solid lines describe the values in the presence of the obstacle, dotted line the region where the massive interstellar cloud is located, and the dashed line the values without obstacle.

in the variables, as one moves out from the x -axis, are shown in Figs. 7, 9 and 10.

Shock waves form when the speed of injection of mass exceeds the sound speed of the surrounding medium [17]. By changing the values of the temperature of the fluid in the region $x \leq 50$, in order to obtain speeds of mass injection of $|\vec{\beta}| = 0.5$, $|\vec{\beta}| = 0.2$, and $|\vec{\beta}| = 0.01$, we can see that the increment of the particle density due to the sweeping of interstellar medium by the shock wave becomes appreciable only for $|\vec{\beta}| = 0.5$ (see Fig. 10). A similar argument applies to the pressure cone (see Fig. 9(a)). Indeed, in the other cases, the speed of mass injection is lower than the sound speed, and therefore no shock-wave can be formed.

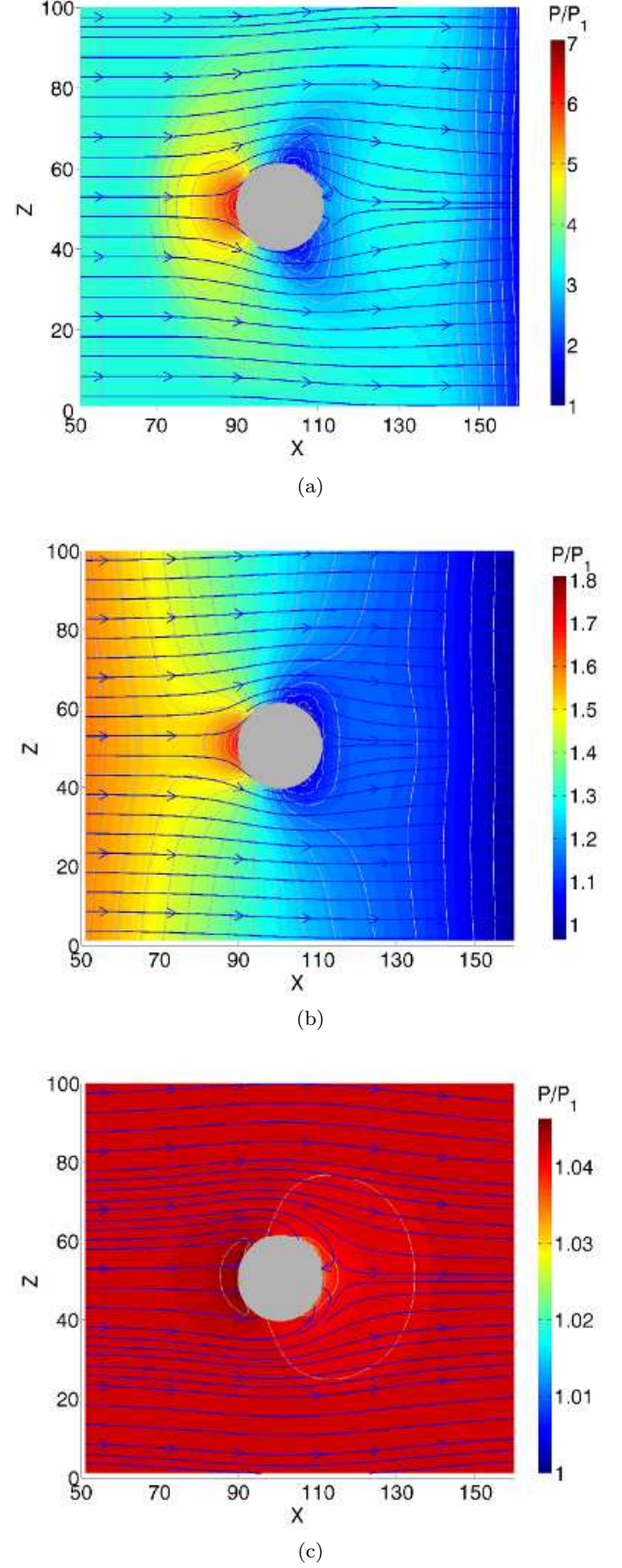


FIG. 9: Fluid pressure after the collision of the shock wave, produced by a supernova explosion, against the massive interstellar cloud, at (a) $|\vec{\beta}| = 0.5$, (b) $|\vec{\beta}| = 0.2$, and (c) $|\vec{\beta}| = 0.01$ in a cut going through the center of the cloud. The streamlines represent the velocity field, and the colors the pressure.

VI. CONCLUSIONS AND OUTLOOK

In this paper, we have provided a detailed discussion of the Lattice Boltzmann formulation for relativistic fluids. In particular, details on the construction of the relevant lattice equilibria are provided, emphasizing the common aspects with standard Lattice Boltzmann theory.

The scheme is shown to exhibit excellent agreement with previous numerical simulations of shock wave propagation in quark-gluon plasmas, at a fraction of the cost of hydrodynamic codes. Near-second order accuracy with grid resolution and linear computational time with space-time resolution, are evidenced.

As an example of relativistic hydrodynamics with non-trivial geometries, we have also applied our scheme to an astrophysical system, namely the collision of a shock wave, produced by a supernova explosion, against a cold molecular cloud. The numerical simulations show good qualitative results yielding information, that can be compared with experimental results and other numerical methods.

For the case of quark-gluon plasma simulations, the present lattice-kinetic algorithm appears to be nearly an order of magnitude faster than corresponding hydrodynamic codes. This is due to the fact that, at variance with any hydrodynamic representation, LB moves information along constant light-cones rather than space-time changing material fluid streamlines [40]. This trivializes the Riemann problem to a mere shift of the distribution function along the corresponding lightcone, a *floating-point free, exact* operation, which is way more convenient than propagating hydrodynamic fields along space-time changing streamlines. Such an advantage, key in ordinary lattice Boltzmann fluids, might be even accrued in the relativistic context.

Several issues remain open for future research. First, extensions of the present scheme to higher-order lattices are worth being considered, for they should give access to higher values of β , by use of correspondingly higher-order lattice equilibria. This strategy has indeed proved very effective for the case of compressible and thermal non-relativistic fluids [41–44].

Another important question concerns the existence of a relativistic lattice H-theorem. Apart from the theoretical interest on its own, this has major implications on the numerical stability of the scheme at high Reynolds number, i.e. for the simulation of relativistic turbulence [45].

Yet another interesting research direction is the simulation of relativistic flows with a non-ideal equation of state, which may find applications in relativistic cosmology and high-energy theories of the early universe [46, 47].

These are just but a few of the many exciting developments and applications which may currently be envisaged for the relativistic Lattice Boltzmann equation presented in this paper.

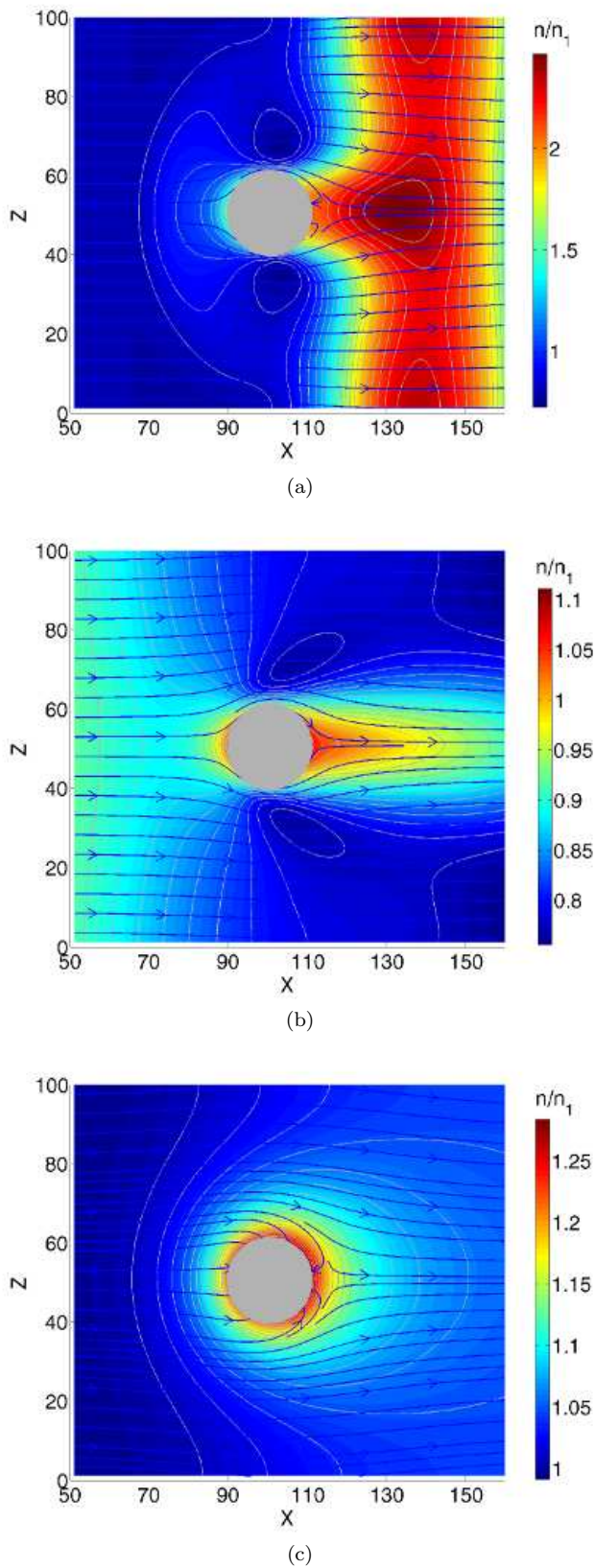


FIG. 10: Particles density of the fluid after the collision of the shock wave, produced by a supernova explosion, against the massive interstellar cloud, at (a) $|\beta| = 0.5$, (b) $|\beta| = 0.2$, and (c) $|\beta| = 0.01$ in a cut going through the center of the cloud. The streamlines represent the velocity field, and the colors the particles density.

Acknowledgments

The authors are grateful to P. Romatsche for many valuable suggestions. SS would like to acknowledge kind hospitality and financial support from ETH Zürich, Tufts University and the Programme "Partial Differential Equations in Kinetic Theories" at the Isaac Newton Institute for Mathematical Sciences, Cambridge, UK.

BB would like to acknowledge NSF grant 0619447, and TeraGrid allocation MCA08X031. MM and HH are grateful for the financial support of the Swiss National Science Foundation (SNF) under Grant No. 116052.

Appendix A: Moment Matching Procedure

To obtain the equilibrium distribution functions f_i^{eq} and g_i^{eq} that reproduce in the continuum limit the hydrodynamic equations, Eqs. (5) and (6), we use the moment-matching procedure. In section III B, we describe the procedure and calculate the equilibrium distribution functions f_i^{eq} in order to obtain the conservation of particle number, Eq. (6). Following a similar procedure, to find the equilibrium distributions g_i^{eq} , first we can write it, as before, as

$$g_i^{\text{eq}} = w_i [C + \vec{c}_i \cdot \vec{D} + \vec{E} : (\vec{c}_i \vec{c}_i - \alpha \vec{I})] \quad , \text{ for } i > 0 \quad , \quad (\text{A1a})$$

$$g_0^{\text{eq}} = w_0 [F] \quad , \quad (\text{A1b})$$

with C , \vec{D} , α , and \vec{E} the Lagrange multipliers. Then, we impose the following constraints:

$$\sum_{i=0}^{18} g_i^{\text{eq}} = \gamma^2 (\epsilon + P) - P \quad , \quad (\text{A2})$$

$$\sum_{i=0}^{18} g_i^{\text{eq}} \vec{c}_i = (\epsilon + P) \gamma^2 \vec{u} \quad . \quad (\text{A3})$$

and additionally,

$$\sum_{i=0}^{18} g_i^{\text{eq}} c_{ia} c_{i\beta} = P \delta_{ab} + (\epsilon + P) \gamma^2 u_a u_b \quad . \quad (\text{A4})$$

Replacing Eq. (A1) into Eq. (A2), (A3), and (A4), and summing up over the index i , we obtain

$$\frac{1}{3} \left(2C + F + \text{Tr}(\vec{E})(c_l^2 - 2\alpha) \right) = \gamma^2 (\epsilon + P) - P \quad , \quad (\text{A5})$$

$$\frac{c_l^2}{3} \vec{D} = (\epsilon + P) \gamma^2 \vec{u} \quad , \quad (\text{A6})$$

and

$$\begin{aligned} \frac{c_l^2}{9} \left(3C + (c_l^2 - 3\alpha) \text{Tr}(\vec{E}) \right) \delta_{ab} + \frac{2c_l^4}{9} E_{ab} &= P \delta_{ab} \\ &+ (\epsilon + P) \gamma^2 u_a u_b \quad , \end{aligned} \quad (\text{A7})$$

where we have defined $\text{Tr}(\vec{E})$ as the trace of the tensor \vec{E} . From Eq. (A6) we can see that $\vec{D} = \frac{3}{c_l^2} (\epsilon + P) \gamma^2 \vec{u}$. If we compare the left and right hand sides of Eq. (A7), we can conclude that $\alpha = \frac{c_l^2}{3}$, and therefore Eq. (A7) is simplified to

$$\frac{c_l^2}{3} C \delta_{ab} + \frac{2c_l^4}{9} E_{ab} = P \delta_{ab} + (\epsilon + P) \gamma^2 u_a u_b \quad . \quad (\text{A8})$$

Comparing again both sides of this equation the Lagrange multipliers $C = \frac{3P}{c_l^2}$ and $E_{ab} = \frac{9}{2c_l^4} (\epsilon + P) \gamma^2 u_a u_b$ are obtained. Now, the only missing parameter to be determined is F . Replacing the values of C , α , and \vec{E} into Eq. (A5), it gives

$$\frac{2P}{c_l^2} + \frac{F}{3} + \frac{c_l^2}{9} \text{Tr}(\vec{E}) = \gamma^2 (\epsilon + P) - P \quad . \quad (\text{A9})$$

From here, we can get the Lagrange parameter F and it can be written as

$$F = (\epsilon + P) \gamma^2 \left[3 - 3 \frac{(2 + c_l^2)P}{c_l^2 (\epsilon + P) \gamma^2} - \frac{3}{2c_l^2} (\epsilon + P) \gamma^2 |\vec{u}|^2 \right] \quad . \quad (\text{A10})$$

Summarizing, we have determined all the Lagrange parameters and therefore the equilibrium distribution functions g_i^{eq} that recover in the continuum limit the conservation equation for the momentum-energy.

Appendix B: Chapman-Enskog Expansion

The discrete Boltzmann equations, Eqs. (22) and (23), determine the evolution of the lattice relativistic fluid. In the continuum limit, these evolution rules must reproduce the partial differential equations of relativistic hydrodynamics. In order to accomplish this task, we adopt a standard Chapman-Enskog expansion. We start by taking the Taylor expansion of the Boltzmann equations, up to second order in spatial and temporal coordinates,

$$\begin{aligned} v_{ia} \partial_a f_i + \frac{1}{2} \sum_{a,b} \partial_a \partial_b f_i v_{ia} v_{ib} + \partial_t f_i \\ + \partial_t v_{ia} \partial_a f_i + \frac{1}{2} \partial_t^2 f_i \delta t^2 = -\frac{1}{\tau} (f_i - f_i^{\text{eq}}) \quad , \end{aligned} \quad (\text{B1a})$$

$$\begin{aligned} v_{ia} \partial_a g_i + \frac{1}{2} \sum_{a,b} \partial_a \partial_b g_i v_{ia} v_{ib} + \partial_t g_i \\ + \partial_t v_{ia} \partial_a g_i + \frac{1}{2} \partial_t^2 g_i \delta t^2 = -\frac{1}{\tau} (g_i - g_i^{\text{eq}}) \quad , \end{aligned} \quad (\text{B1b})$$

where $a, b = x, y, z$ denote the x , y and z components. Next, we expand the distribution functions, and the space-time derivatives in a power series of the Knudsen number κ , as follows:

$$f_i = f_i^{(0)} + \kappa f_i^{(1)} + \kappa^2 f_i^{(2)} + \dots \quad , \quad (\text{B2a})$$

$$g_i = g_i^{(0)} + \kappa g_i^{(1)} + \kappa^2 g_i^{(2)} + \dots \quad , \quad (\text{B2b}) \quad \text{and}$$

$$\partial_t = \kappa \partial_{t_1} + \kappa^2 \partial_{t_2} + \dots \quad , \quad (\text{B2c})$$

$$\partial_a = \kappa \partial_{1a} + \kappa^2 \partial_{2a} \dots \quad . \quad (\text{B2d})$$

It is assumed that only the 0th order terms of the distribution functions contribute to the macroscopic conserved variables. Therefore, for $n > 0$ we have

$$\sum_i f_i^{(n)} = 0 \quad , \quad \sum_i g_i^{(n)} = 0 \quad , \quad (\text{B3a})$$

$$\sum_i f_i^{(n)} \vec{v}_i = 0 \quad , \quad \sum_i g_i^{(n)} \vec{v}_i = 0 \quad . \quad (\text{B3b})$$

By inserting these results into Eqs.(B1a) and (B1b), we obtain at 0th-order in κ

$$f_i^{\text{eq}} = f_i^{(0)} \quad , \quad (\text{B4})$$

$$g_i^{\text{eq}} = g_i^{(0)} \quad , \quad (\text{B5})$$

to the first order in κ ,

$$v_{ia} \partial_{1a} f_i^{(0)} + \partial_{t_1} f_i^{(0)} = -\frac{f_i^{(1)}}{\tau} \quad , \quad (\text{B6a})$$

$$v_{ia} \partial_{1a} g_i^{(0)} + \partial_{t_1} g_i^{(0)} = -\frac{g_i^{(1)}}{\tau} \quad , \quad (\text{B6b})$$

and to the second order in κ ,

$$\left(1 - \frac{1}{2\tau}\right) (v_{ia} \partial_{1a} + \partial_{t_1}) f_i^{(1)} + \partial_{t_2} f_i^{(0)} + v_{ia} \partial_{2a} f_i^{(0)} = -\frac{f_i^{(2)}}{\tau} \quad . \quad (\text{B7a})$$

$$\left(1 - \frac{1}{2\tau}\right) (v_{ia} \partial_{1a} + \partial_{t_1}) g_i^{(1)} + \partial_{t_2} g_i^{(0)} + v_{ia} \partial_{2a} g_i^{(0)} = -\frac{g_i^{(2)}}{\tau} \quad . \quad (\text{B7b})$$

A this stage, all the ingredients required to determine the equations that the model satisfies in the continuum limit, are available. By summing up Eqs. (B6a), (B6b), (B7a), and (B7b) over index i , taking into account Eqs. (B4), (B5), and the equilibrium distribution functions defined by Eqs. (37), (38), and (39), we obtain

$$\partial_{t_1}(n\gamma) + \partial_{1a}(n\gamma u_a) = 0 \quad , \quad (\text{B8})$$

$$\partial_{t_1}((\epsilon + P)\gamma^2 - P) + \partial_{1a}((\epsilon + P)\gamma^2 u_a) = 0 \quad , \quad (\text{B9})$$

$$\partial_{t_2}(n\gamma) + \partial_{2a}(n\gamma u_a) = 0 \quad . \quad (\text{B10})$$

$$\partial_{t_2}((\epsilon + P)\gamma^2 - P) + \partial_{2a}((\epsilon + P)\gamma^2 u_a) = 0 \quad . \quad (\text{B11})$$

By adding these equations, the first and second scalar equations, associated with the conservation of the number of particle and the first conservation equation for the momentum-energy,

$$\partial_t(n\gamma) + \partial_a(n\gamma u_a) = 0 \quad , \quad (\text{B12})$$

and

$$\partial_t((\epsilon + P)\gamma^2 - P) + \partial_a((\epsilon + P)\gamma^2 u_a) = 0 \quad , \quad (\text{B13})$$

are obtained, which correspond to Eqs.(36) and (35a), respectively. To derive the second conservation equation, Eq.(35b), the equations (B6b) and (B7b) must be multiplied by \vec{v}_i and summed up over the index i , which leads to

$$\partial_{t_1}[(\epsilon + P)\gamma^2 u_b] + \partial_{1b}P + \partial_{1a}[(\epsilon + P)\gamma^2 u_a u_b] = 0 \quad , \quad (\text{B14})$$

and

$$\partial_{t_2}[(\epsilon + P)\gamma^2 u_b] + \partial_{2b}P + \partial_{2a}[(\epsilon + P)\gamma^2 u_a u_b] + \partial_{1a}\Pi_{ab}^{(1)} = 0 \quad , \quad (\text{B15})$$

where the first order tensor $\Pi_{ab}^{(1)} = (1 - \frac{1}{2\tau}) \sum_i g_i^{(1)} v_{ia} v_{ib}$ is defined. By replacing the distribution function $f_i^{(1)}$ from Eq.(B6b) into the tensor $\Pi_{ab}^{(1)}$, and the result into Eq.(B15), we obtain

$$\partial_{t_2}[(\epsilon + P)\gamma^2 u_b] + \partial_{2b}P + \partial_{2a}[(\epsilon + P)\gamma^2 u_a u_b] - \partial_{1a}[\partial_{1b}(\eta\gamma u_a) + \partial_{1a}(\eta\gamma u_b) + \partial_{1l}(\eta\gamma u_l)\delta_{ab}] = 0 \quad , \quad (\text{B16})$$

with the viscosity $\eta = \frac{1}{3}\gamma(\epsilon + P)(\tau - \delta t/2)c_l^2$, l denoting again the spatial components. To arrive to these results, we have assumed low-speed, $|\vec{u}| \ll c$. The second momentum-energy conservation equation, Eq.(35b), is obtained by summing up Eqs.(B16) and (B14). It gives

$$\partial_t[(\epsilon + P)\gamma^2 u_b] + \partial_b P + \partial_a[(\epsilon + P)\gamma^2 u_a u_b] - \partial_a[\partial_b(\eta\gamma u_a) + \partial_a(\eta\gamma u_b) + \partial_l(\eta\gamma u_l)\delta_{ab}] = 0 \quad . \quad (\text{B17})$$

The derivation of the dissipative term associated with the viscosity η , in Eq. (B17), is obtained assuming low values of β to neglect higher order terms ($\sim |\vec{u}|^3$) contributions.

Summarizing, Eqs. (B12), (B13) and (B17) determine the evolution of the fluid, according to the relativistic hydrodynamics equations.

-
- [1] M. Mendoza, B. Boghosian, H. Herrmann, and S. Succi, Phys. Rev. Lett. **105**, 014502 (2010).
- [2] A. Dolezal and S. S. M. Wong, J. of Comput. Phys. **120**, 266 (1995).
- [3] D. S. Balsara, J. of Comput. Phys. **114**, 284 (1994).
- [4] V. Schneider, U. Katscher, D. H. Rischke, B. Waldhauser, and J. A. Maruhn, J. of Comput. Phys. **105**, 92 (1993).
- [5] J. Yang, M. Chen, I. Tsai, and J. Chang, J. of Comput. Phys. **136**, 19 (1997).
- [6] S. Succi and R. Benzi, Physica D **69** 3-4, 327 (1993).
- [7] S. Succi, G. Amati, and R. Piva, Int. J. Mod. Phys. C **8**, 869 (1997).
- [8] S. Wolfram, Journal of Statistical Physics **45**, 471 (1986), ISSN 0022-4715, URL <http://dx.doi.org/10.1007/BF01021083>.
- [9] X. He and L.-S. Luo, Phys. Rev. E **56**, 6811 (1997).
- [10] J. Adams *et al.* [STAR Collaboration], Phys. Rev. Lett. **91**, 172302 (2003).
- [11] A. Adare *et al.* [PHENIX Collaboration], Phys. Rev. Lett. **101**, 232301 (2008).
- [12] F. Wang [STAR Collaboration], J. Phys. G **30**, S1299 (2004).
- [13] J. Adams *et al.* [STAR Collaboration], Phys. Rev. Lett. **95**, 152301 (2005).
- [14] J. G. Ulery [STAR Collaboration], Nucl. Phys. A **774**, 581 (2006).
- [15] N. N. Ajitanand [PHENIX Collaboration], Nucl. Phys. A **783**, 519 (2007).
- [16] A. Adare *et al.* [PHENIX Collaboration], Phys. Rev. C **78**, 014901 (2008).
- [17] C. McKee and B. Draine, Science **252**, 397 (1991).
- [18] R. A. Chevalier, Nature **355**, 691 (1992).
- [19] A. M. Soderberg *et al.*, Nature Letters **463**, 513 (2010).
- [20] A. M. Soderberg *et al.*, Nature Letters **442**, 1014 (2006).
- [21] I. Bouras, E. Molnar, H. Niemi, Z. Xu, A. El, O. Fochler, C. Greiner, and D. H. Rischke, Phys. Rev. Lett. **103**, 032301 (2009).
- [22] M. Müller, J. Schmalian, and L. Fritz, Phys. Rev. Lett. **103**, 025301 (2009).
- [23] C. Cercignani and G. M. Kremer, *The Relativistic Boltzmann Equation: Theory and Applications* (Boston; Basel; Berlin: Birkhauser, 2002).
- [24] R. Baier, P. Romatschke, D. T. Son, A. O. Starinets, and M. A. Stephanov, JHEP **4** (2008).
- [25] C. Marle, C. R. Acad. Sc. Paris **260**, 6539 (1965).
- [26] M. Takamoto and S. Inutsuka, Accepted to publication in Physica A (2010).
- [27] J. Anderson and H. Witting, Physica **74**, 466 (1974).
- [28] S. Chen and G. Doolen, Annu. Rev. Fluid Mech. **30**, 329 (1998).
- [29] P. Bhatnagar, E. P. Gross, , and M. Krook, Phys. Rev. **94**, 511 (1954).
- [30] S. Succi, *The Lattice Boltzmann Equation for Fluid Dynamics and Beyond* (Oxford University Press, USA, 2001), ISBN 0198503989.
- [31] J. Boris, Ann. Rev. Fluid Mech. **21**, 345 (1989).
- [32] B. M. Boghosian, P. Love, P. V. Coveney, S. Succi, I. Karlin, and J. Yezpez, Phys. Rev. E Rapid Communications **68**, 025103 Part 2 (2003).
- [33] I. V. Karlin, A. Ferrante, and H. C. ttinger, EPL (Europhysics Letters) **47**, 182 (1999).
- [34] F. J. Higuera, S. Succi, and R. Benzi, EPL (Europhysics Letters) **9**, 345 (1989), URL <http://stacks.iop.org/0295-5075/9/i=4/a=008>.
- [35] D. d'Humières, Rarefied Gas Dynamics: Theory and Simulations **159**, 450 (1992).
- [36] Z. Xu and C. Greiner, Phys. Rev. C **71**, 064901 (2005).
- [37] L. F. Richardson, Philosophical Transactions of the Royal Society of London. Series A, Containing Papers of a Mathematical or Physical Character **210**, 307 (1911), <http://rsta.royalsocietypublishing.org/content/210/459-470/307.full.pdf+html>, URL <http://rsta.royalsocietypublishing.org/content/210/459-470/>
- [38] L. F. Richardson and J. A. Gaunt, Philosophical Transactions of the Royal Society of London. Series A, Containing Papers of a Mathematical or Physical Character **226**, 299 (1927), <http://rsta.royalsocietypublishing.org/content/226/636-646/299.full.pdf+html>, URL <http://rsta.royalsocietypublishing.org/content/226/636-646/>
- [39] R. Benzi, S. Succi, and M. Vergassola, Phys. Rep. **222**, 145 (1992).
- [40] P. Romatsche, private communication. <http://hep.itp.tuwien.ac.at/~paulrom/>.
- [41] F. J. Alexander, H. Chen, S. Chen, and G. D. Doolen, Phys. Rev. A **46**, 1967 (1992).
- [42] C. Sun and A. T. Hsu, Phys. Rev. E **68**, 016303 (2003).
- [43] H. Yu and K. Zhao, Phys. Rev. E **61**, 3867 (2000).
- [44] F. Chen, A. Xu, G. Zhang, Y. Li, and S. Succi, EPL (Europhysics Letters) **90**, 54003 (2010), URL <http://stacks.iop.org/0295-5075/90/i=5/a=54003>.
- [45] M. J. Korpi, A. Brandenburg, A. Shukurov, I. Tuominen, and . Nordlund, The Astrophysical Journal Letters **514**, L99 (1999), URL <http://stacks.iop.org/1538-4357/514/i=2/a=L99>.
- [46] P. Romatschke, Int. J. Mod. Phys. E **19**, 1 (2009).
- [47] M. Cheng, N. H. Christ, S. Datta, J. van der Heide, C. Jung, F. Karsch, O. Kaczmarek, E. Laermann, R. D. Mawhinney, C. Miao, et al., Phys. Rev. D **77**, 014511 (2008).